Multi-technique approach for estimating groundwater transit time through the saturated zone of an unconfined granular aquifer

Chaima Miled[1,2*], Romain Chesnaux[1,2], Julien Walter[1,2], Lamine Boumaiza[3], Maxime C. Paré[4]

[*]Corresponding author: chaima.miled1@uqac.ca

[1] Département des Sciences Appliquées, Université du Québec à Chicoutimi, Saguenay (Québec), G7H 2B1, Canada

[2] Centre d'études sur les ressources minérales, Groupe de recherche Risque Ressource Eau, Saguenay (Québec), G7H 2B1, Canada

[3] Department of Earth and Environmental Sciences, University of Waterloo, Waterloo (Ontario), N2T 0A4, Canada

[4] Département des Sciences Fondamentales, Laboratoire sur les écosystèmes terrestres boréaux (EcoTer), Université du Québec à Chicoutimi, Saguenay (Québec), G7H 2B1, Canada

Abstract

Agricultural activities can generate contaminants that enter underlying granular aquifers and become transported within the aquifer to adjacent streams. Here, we estimate the transit time of groundwater through a saturated granular unconfined aquifer in an agricultural region of Saguenay-Lac-Saint-Jean, Quebec (Canada). We apply a multi-technique approach—integrating analytical, hydrogeochemical, and numerical methods—to determine groundwater flow from a recharge (wetland) to discharge zone (groundwater seep). Fieldwork observations, including borehole drilling, soil/groundwater sampling, and piezometers, were combined with laboratory measurements of soil hydrogeological properties and stable ($\delta^{18}O_{H2O}$ and $\delta^{2}H_{H2O}$)/radioactive (^{3}H) isotopes in the collected groundwater. Our Dupuit–Forchheimer-based analytical method estimated a groundwater transit time of 7.75 years, whereas our hydrogeochemical-based and 3D FEFLOW numerical method produced estimates of 7.34 years and 7.27 years, respectively. The similarity of the three estimates highlights the robustness of our approach, which integrates field data to produce accurate assessments of groundwater transit time. This multi-technique approach will help in the sustainable management of groundwater resources and for preparing effective environmental plans for agricultural practices in areas underlain by aquifers.

Keywords: Analytical solution, Groundwater recharge, Hydrogeochemistry, Quebec, Tritium, Water table

1. Introduction

Groundwater plays an integral role in the water cycle by connecting surface water ecosystems, contributing to river and stream flows, and irrigating food resources used by terrestrial fauna (Boumaiza et al. 2020c; Ritter 2002; Zedler and Kercher 2005). When contaminants are released into the subsurface, mechanisms such as advection, dispersion, and diffusion transport the introduced substance within the aquifer over distances of several meters to tens of kilometers (Bradley 2013; Gorelick et al. 1993). The amount of contaminant transported into the subsurface depends on the nature of the contaminant, the aquifer's geology, and groundwater flow (Boumaiza et al. 2022a; McCarthy and Zachara 1989). The transit time of the contaminant can be defined in two ways. First, transit time through the aquifer vadose zone represents the time required for the contaminant to reach the water table from the ground surface (Sousa et al. 2013). The second concept refers to the transit time of a parcel of water from its recharge at the water table to its discharge along a stream bed or spring (Cartwright and Morgenstern 2016). Knowing the transit time of a contaminant permits evaluating the potential movement of groundwater contamination.

Over the past few decades, considerable research has been devoted to investigating groundwater transit times (Boumaiza et al. 2021a; McGuire and McDonnell 2006). Isotopic signatures have been used effectively to trace groundwater transit in aquifers. For example, Małoszewski et al. (1983); (Vitvar and Balderer 1997) used water isotopic content ($\delta^{18}O_{H2O}$ and $\delta^{2}H_{H2O}$) and solute data in precipitation and stream water to estimate transit time. These studies were limited however by (i) the poor quality of the data series, (ii) the short length of the observational record, and (iii) the sample collection strategy. The application of natural tracers to determine groundwater circulation is widely documented (Clark and Fritz

1997; Cook and Herczeg 2012; Mazor 2003). Some environmental tracers such as carbon-14 (^{14}C) and tritium (^{3}H) are used to estimate groundwater transit time, whereas other tracers can reveal the origin of flows, groundwater mixing, and mineralization (Fontes 1992). Tritium (^{3}H) has been used to determine the transit times of shallow groundwater, soil water, and surface water (Cartwright and Morgenstern 2015, 2016; Cook and Böhlke 2000). When ^{3}H activity is combined with models that describe the distribution of flow paths within an aquifer (Cook and Böhlke 2000), transit time estimates, up to ~100 years old, can be provided for groundwater.

Multi-tracer approaches have been widely used over the last two decades (Ekwurzel et al. 1994; Gillon et al. 2012; Lefebvre et al. 2015; Mazariegos et al. 2017). Applying several tracers allows identifying groundwater processes (e.g., mixing processes, dispersion, degradation, contamination) that could have been misinterpreted or not observed through use of a single tracer.

Furthermore, the continual development of analytic expressions has made it possible to describe horizontal and vertical flow velocities, age profiles, and fluxes such as recharge (Chesnaux 2013; Chesnaux et al. 2021; Cook and Böhlke 2000; Vogel 1967). One of the earliest models was that of Vogel (1967) which provided a solution based on Darcy's Law for the vertical distribution of hydraulic age in an unconfined aquifer characterized by uniform recharge and constant thickness. Cook and Böhlke (2000) summarized the range of analytical solutions available for determining hydraulic age. However, these analytical solutions are only required for homogeneous flow systems. Analytical models can also now

combine a hydraulic simulation with an advection–dispersion solution to describe tracer movements within groundwater flow (Bethke and Johnson 2008; Leray et al. 2012).

Multiple numerical methods are available for estimating groundwater travel times (Cornaton 2003; Goode 1996). Goode (1996) applied a numerical advective–dispersive transport model to derive an equation for determining groundwater age and groundwater mass. Cornaton (2003); Etcheverry and Perrochet (2000) applied residence time theory to produce deterministic models of groundwater age. Despite being widely applicable, numerical techniques for solving groundwater transit time require more computational resources; however, they are appropriate for modeling more complex aquifer systems.

Many studies have focused on estimating groundwater transit time using a single approach, whereas few have tried to combine different approaches (Basu et al. (2012). Although necessary for effective and sustainable groundwater management, studies combining different approaches are challenging because the multiple sources of input data require diverse measurements from relatively large aquifers. Hence, the collection of required field data is one of the most expensive, albeit valuable, tasks for estimating groundwater transit time.

This field-based study applies a multi-technique approach to estimate groundwater transit time through an unconfined granular aquifer. Our approach integrates (i) an analytical-based solution, developed by Chesnaux et al. (2005) to calculate groundwater travel times in the configuration of a Dupuit–Forchheimer type flow system (Bear 1972b; Bear 1988; Dupuit 1863; Forchheimer 1886b) in an unconfined aquifer, (ii) a hydrogeochemical technique involving environmental tracers ($\delta^{18}O_{H2O}$, $\delta^{2}H_{H2O}$, and ^{3}H), and (iii) numerical

modeling for which field observations are used to calibrate the developed model. We selected the aquifer lying within an agricultural experimental site, *Bleuetière d'Enseignement et de Recherche* (BER) because agricultural practices can generate contaminants that are transported through the granular aquifer to reach the surrounding rivers. Note that there are no pumping activities, nor irrigation, nor other possible human activities that may influence recharge on this site. Collected field data from BER combined with diverse techniques heightens the accuracy of transit time estimates. This improved estimate is valuable for groundwater researchers/managers for preparing effective environmental plans for agricultural regions.

This study aims to characterize the BER site's aquifer, undergoing commercial wild blueberry activity, by (i) estimating groundwater recharge and (ii) evaluating the transit time of groundwater through the aquifer system.

2. Materials and methods

2.1. Study area

BER is an experimental scientific research site managed by the Université du Québec à Chicoutimi (Fig. 1). The site is located 10 km southwest of the town of Normandin in the Saguenay-Lac-Saint-Jean region (SLSJ) of Quebec, Canada. The 55-ha study site is an agricultural field covered by wild blueberries crops (*Vaccinium angustifolium* Aiton and *Vaccinium myrtilloides* Michx). Regional climate is characterized by hot, humid summers, cold, snowy winters, and wet springs and autumns. Mean annual precipitation is approximately 967 $mm \cdot yr^{-1}$. Average temperatures range from −15.2 °C in winter to 18.9 °C in summer (Gouv.qc 2022).

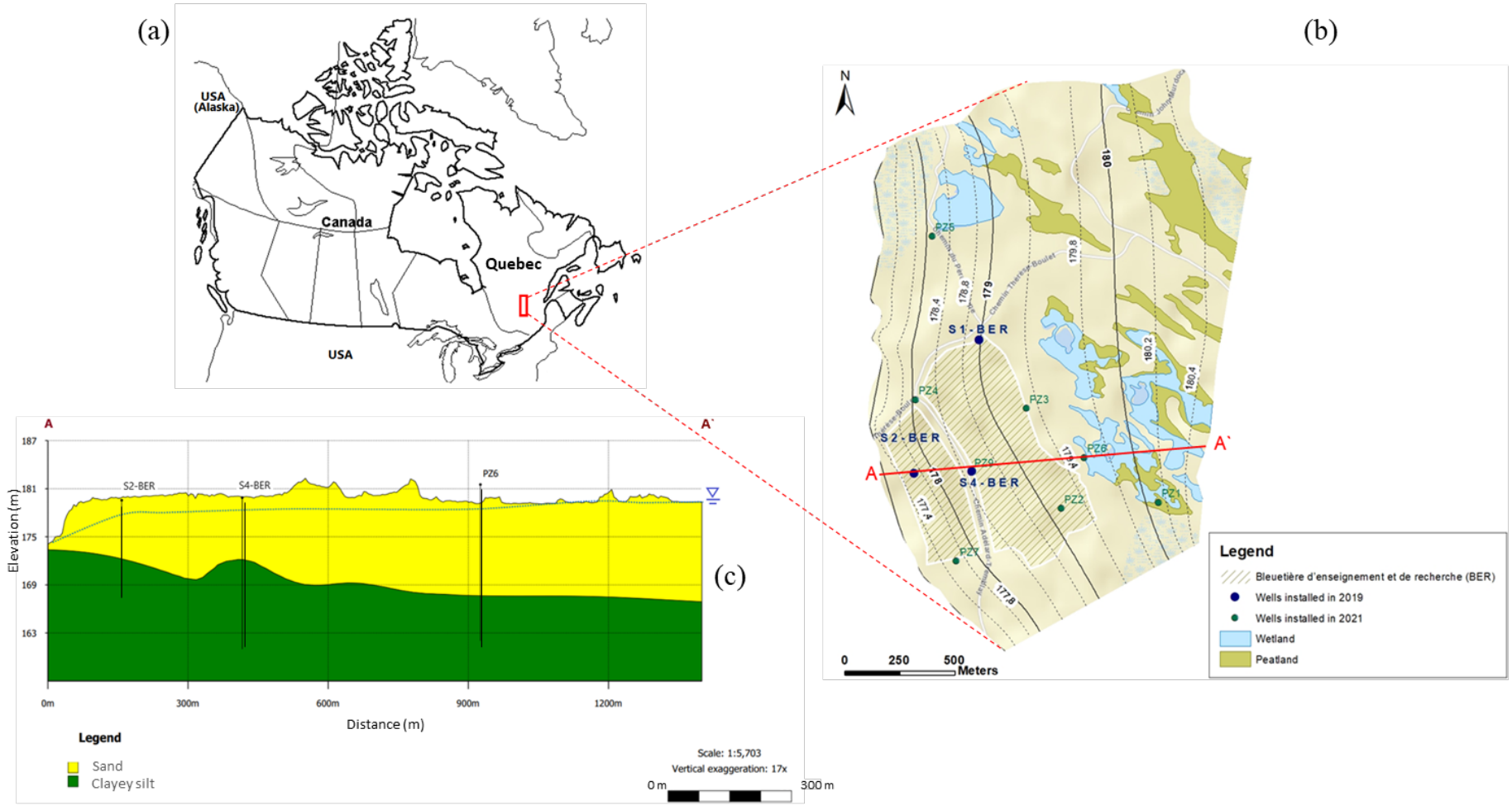

Fig. 1. **a**) Location of the study site in Québec (Canada); **b**) locations of the installed observation wells, showing the location of the cross-section presented in c), the surface cover, and equipotential lines; **c**) stratigraphic cross-section A–A′ with subsurface materials and the location of studied wells.

129 BER lies on unconsolidated Quaternary deposits that overlie the crystalline bedrock of the
130 Grenville Province. The Quaternary sediments date to the last glacial and deglacial period.
131 Following the retreat of the Laurentide ice sheet about 11,800 years ago, the Laflamme Sea
132 inundated much of the SLSJ region (LaSalle and Tremblay 1978), leaving deep water
133 marine deposits consisting of grey clay or clayey silt. The BER aquifer—maximum
134 thickness of 14 m—comprises proglacial deltaic sands and silt deposited over an aquitard
135 composed of clayey silt from the Laflamme Sea (Fig. 1). The surface of the unconfined
136 aquifer is characterized by a relatively flat topography, wetlands in the eastern portion of
137 the BER, and a thin vadose zone of variable thickness, 0.5–2.5 m below ground surface
138 (bgs).

139 **2.2. Field sampling and laboratory analyses**

140 *2.2.1. Soil sampling*

141 Three boreholes were drilled at the study site in October 2019 to serve as the observation
142 wells S1-BER, S2-BER, and S4-BER with depths of 8.23, 6.71, and 12.19 m bgs,
143 respectively (Courchesne 2019). In July 2021, four additional boreholes (PZ-1, PZ2, PZ3,
144 and PZ4) were drilled to a maximum depth of 5 m using a hand threshing beating auger
145 and were then equipped with observation well installations (Fig. 1).

146 During borehole drilling, continuous soil samples were collected from the split-spoon
147 sampler (0.69-m-long, 0.05-m-diameter). These soil samples were collected at an average
148 interval of 20 cm to obtain a high-resolution vertical profile. At each sampling, the split
149 spoon was cleaned using dry towels to minimize intersample contamination. Following a
150 visual description (sediment texture, colour, humidity) of the samples in the field, the

collected samples were quickly stored in separately labelled polyethylene Ziploc© bags, tightly sealed to avoid moisture loss through evaporation.

2.2.2. Soil physical properties by drying

In the laboratory, all fresh soil samples were placed into individual metal cylinders of known weight and volume. Following their weighing, the soil samples were dried in an oven for 48 h at 105 °C. The dried-sample weight was then used to determine the total wet and dry soil mass. Gravimetric water content (GWC, expressed in %) was calculated for each soil sample (Gardner 1965). Dry bulk density (D_b), expressed in g·cm^{-3}, was determined according to Black (1965) and the volumetric water content (VWC, expressed in %) was calculated following (Gardner 1965) and assuming a water density (ρ_w) of 1 g·cm^{-3}. Soil porosity (n, expressed in %) was calculated using Black (1965)and assuming a particle density (ρ_p) of 2.69 g·cm^{-3} for sand (Boumaiza et al. 2015, 2017; Boumaiza et al. 2020b). The void ratio (e) was also determined. We used n and e to estimate the saturated hydraulic conductivity (Ks).

2.2.3. Soil physical properties by grain size

Successive soil samples of similar texture and structure were combined into a single sample. These grouped samples were analysed with grain-size sieves, and grain-size fractions were reported following the Wentworth classification (Wentworth 1922) and plotted as granulometric curves. The latter were used to estimate Ks using five empirical equations (i.e., Hazen (1983), Beyer (1964), Chapuis (2004), Sauerbrey (1932), U.S. Bureau of Reclamation (Milan and Andjelko 1992), and Navfac (1974). These equations and their application limits are detailed in Table 1. Some empirical equations adopted in our study

may not apply to certain soil samples because of different conditions of applicability related to void ratio and granulometry. Accordingly, we calculated *K*s for each soil sample using only the applicable empirical equations and adopted a geometric mean value (Boumaiza et al. 2020a; Zappa et al. 2006). An equivalent saturated hydraulic conductivity (*K.eq*) value was determined for the full soil profile of each drilled borehole.

Table 1. Selected empirical equations used to estimate *K*s and the conditions necessary for their application

Method	Empirical formula for *Ks* ($cm \cdot s^{-1}$)	Applicability conditions
Hazen	$(d_{10})^2$ with d_{10} in mm	1. Sand and gravel 2. $C_u \leq 5$ 3. 0.1 mm $\leq d_{10} \leq$ 3 mm
Chapuis	$2.4622((d_{10})^2 e^3)/ (1 + e))^{0.7825}$ with d_{10} in mm	1. All natural soils without plasticity 2. 0.003 mm $\leq d_{10} \leq$ 3 mm 3. $0.3 \leq e \leq 1$
Sauerbrey	$2.436n^3 (d_{17})^2/ (1 - n)^2$ with d_{17} in mm	1. Sand and silty sand 2. d10 $\leq$ 0.5 mm
Beyer	$0.45(d_{10})^2 \log(500/C_u)$ with d_{10} in mm	1. Sand 2. 0.06 mm $\leq d_{10} \leq$ 0.6 mm 3. $1 \leq C_u \leq 20$
USBR	$0.36(d_{20})^{2.3}$ with d_{20} in mm	1. Sand and gravel 2. $C_u \leq 5$
NAVFAC DM7	$(d_{10})^{1.291e-0.6435}$ $(d_{10})^{0.5504e-02937}$ with d_{10} in mm	1. Sand and mixtures of sand and gravel 2. $2 \leq C_u \leq 12$ 3. $d_{10}/ d_5 \leq$ 3 mm

dx: effective grain size of x (% by weight of soil)
Cu: coefficient of uniformity for non-plastic soils (Cu = d10/d60)

2.3. Groundwater sampling and isotope analyses

The groundwater sampling program included groundwater samples collected from four observation wells, PZ-6, S1-BER, S2-BER, and S4-BER, for isotope analyses (Fig. 1). Prior to sampling, stagnant groundwater present in the observation wells was purged using a pumping system. The physicochemical parameters—temperature (T), pH, and electrical

conductivity (EC)—of the pumped groundwater were then monitored with a portable multi-parameter probe until three consecutive readings stabilized within ±10%. Once stable results were attained, groundwater samples were then collected. Groundwater destined for $\delta^{2}H_{H2O}$ and $\delta^{18}O_{H2O}$ analyses was collected in two 30 mL high-density polyethylene (HDPE) bottles, and water for ^{3}H activity was collected in 2000 mL HDPE bottles. All samples were collected in bottles without headspace and fitted with Teflon septa parafilm-caps to prevent evaporation. The groundwater samples were stored in a cooler at 4 °C during fieldwork before being stored in a refrigerator. All groundwater samples were transported to the Environmental Isotope Laboratory (EIL) at the University of Waterloo, Ontario, Canada.

The $\delta^{2}H_{H2O}$ and $\delta 18O_{H2O}$ ratios were determined using a Los Gatos Research Triple Liquid Water Isotope Analyzer LGR T-LWIA 45-EP following the analytical scheme recommended by the International Atomic Energy Agency (IAEA) (Penna et al. 2010). Groundwater samples for ^{3}H were degassed and stored in dedicated glass bulbs for the accumulation of the tritium decay product. For high-precision analyses, samples were enriched (ultra-low levels) 45–50× by electrolyzing multiple additions of sample followed by counting. The detection limit of ultra-low-level enriched samples is 0.1 ± 0.1 TU (1 TU equals a radioactivity concentration of 0.118 $Bq \cdot L^{-1}$) at 2 sigma (at low levels) (Taylor 1976). The obtained ^{3}H activities were corrected for radioactive decay back to the time of the precipitation event, and ^{3}H activities are expressed in tritium units (TU). The isotope ratios, expressed in permil (‰) using delta (δ) notation, were calculated using Eq.1, where R_{sample} and $R_{standard}$ are the sample's and the standard's ratios, respectively, of the heavier to lighter isotope, i.e., $^{2}H/^{1}H$, $^{15}N/^{14}N$, or $^{18}O/^{16}O$.

$$\delta = \left(\frac{R_{\text{sample}} - R_{\text{standard}}}{R_{\text{sample}}} \right) \times 1000 \, . \quad (1)$$

Both $\delta^{2}H_{H2O}$ and $\delta^{18}O_{H2O}$ were reported relative to the Vienna standard mean ocean water (VSMOW), and the precision of the analytical instrument was generally better than ±0.8‰ for $\delta^{2}H_{H2O}$ and ±0.2‰ for $\delta^{18}O_{H2O}$. The distribution of $\delta^{2}H_{H2O}$ and $\delta^{18}O_{H2O}$ of the collected groundwater samples was compared to the range of the local meteoric water line (LMWL) derived from the local precipitation stable isotope data collected during the PACES program (*Programme d'acquisition de connaissances sur les eaux souterraines*).

2.4. Estimating groundwater recharge

We estimated groundwater recharge using the analytical approach developed by Bear (1972b), an approach successfully applied by Chesnaux (2013) and Labrecque et al. (2020). Bear (1972b) approach is based on the Dupuit–Forchheimer model (Dupuit 1863; Forchheimer 1886b), which simplifies groundwater flows to a single dimension by assuming (i) the aquifer overlies a fully horizontal impervious substratum; (ii) the aquifer is bound by two fixed-head boundaries; (iii) the vertical component of groundwater velocity is neglected; and (iv) the aquifer is considered homogeneous and isotropic, and steady-state conditions are assumed for the flow. This analytical approach relies on the general Bear's (Bear 1972b) solution to Dupuit–Forchheimer`s systems for the saturated groundwater thickness above the datum represented by the top of the impervious substratum underlying the aquifer. The solution is expressed as Eq. 2:

$$h(x) = \sqrt{-\frac{W}{k}x^{2} + \left(\frac{h_{L}^{2} - h_{0}^{2}}{L} + \frac{WL}{K} \right) x + h_{0}^{2}} \, . \quad (2)$$

where h is the phreatic surface elevation, x represents the distance from the upstream aquifer boundary, L is the length of the aquifer [L], h_0 and h_L are the fixed upstream (x = 0) and downstream (x = L) heads, respectively (it is assumed that $h_0 > h_L$), K is the hydraulic conductivity of the aquifer [$L \cdot T^{-1}$], and h(x) is the hydraulic head [L] along the x-axis.

The squared saturated thickness of the aquifer where the piezometers were installed was plotted as a function of distance along the flow line (A–A′). The hydraulic head in the aquifer can be calculated by applying a quadratic regression on the plot using Eq. 2. Introducing the estimated *K*eq value into Eq. 2 permits calculating groundwater recharge from the constant coefficient of the polynomial regression model (Chesnaux 2013; Labrecque et al. 2020).

We validated groundwater recharge analytical solution–based estimates using the water table fluctuation (WTF) method (Lanini and Caballero 2021; Lanini et al. 2016). Piezometric fluctuations were monitored between March 2021 and March 2022 at three observation wells (S1-BER, S2-BER and S4-BER). These wells were equipped with pressure sensors to monitor local fluctuations of the water table at 15 min intervals. The ESPERE program includes several commonly used tools to run simultaneously for estimating groundwater recharge. In ESPERE, the WTF is based on the RISE method described by Healy and Cook (2002), assuming a continuous aquifer drainage on an event basis as suggested by Nimmo et al. (2015). The annual groundwater recharge estimated by the WTF-based method equals the sum of all increases in water table level and corrections during the year; it is estimated using Eq. 3.

$$R = Sy \sum(\Delta h + \delta) , \quad (3)$$

where R is the groundwater recharge (mm·year^{-1}), S_y represents the specific yield, $\boldsymbol{\delta}$ is the interpolated exponential recession, and $\Delta \boldsymbol{h}$ is the head defined by the water level rise (D_H) over the time (D_t).

2.5. Estimating groundwater transit time

2.5.1. Analytical approach

We assessed travel time analytically using a closed-form analytical solution developed by Chesnaux et al. (2005). This analytical solution considers the configuration of an unconfined aquifer under Dupuit–Forchheimer conditions (Bear 1972a; Forchheimer 1886a) assuming a steady-state regime, saturated flow through a horizontal aquifer experiencing a constant groundwater recharge, and groundwater discharge to a downgradient fixed-head boundary. Chesnaux et al. (2005) considered two cases: Case I applies to flow systems containing a flow divide between two fixed-head boundaries, whereas Case II refers to unidirectional flow between an upstream and downstream constant head boundary. We adopted Case II (Fig. 2). A transformation was applied to the flow system by placing the upstream head, i.e., the upgradient water divide (see Fig. 2), at the origin of the flow system. The application of Case II is constrained between x = 0 and x = L; however, the solution transformed the flow system between x = |xWD| and x = L + |xWD|, where L + |xWD| = L′, and L′ represents the length of the transformed flow system. Accordingly, the travel time is only representative of the original flow system between x = |xWD| and x = L′. Equation 3 represents the analytical solution developed by Chesnaux et al. (2005), where *K* is the hydraulic conductivity of the aquifer [L·T^{-1}], W is the aquifer

recharge [$L \cdot T^{-1}$], L′ is the length of the aquifer [L], n_e is the effective porosity of the aquifer, and $h_{L'}$ is the constant head boundary discharge [L]. The prefix α in Eq. 5 is calculated using Eq. 4.

$$t(x) = n_e \sqrt{\frac{\alpha}{K \cdot W}} \left[x \sqrt{\frac{1}{x^2} - \frac{1}{\alpha}} - x_i \sqrt{\frac{1}{x^2} - \frac{1}{\alpha}} + \ln \left(\frac{\sqrt{\frac{\alpha}{x_i}} + \sqrt{\frac{\alpha}{x_i^2} - 1}}{\sqrt{\frac{\alpha}{x}} + \sqrt{\frac{\alpha}{x^2} - 1}} \right) \right], \quad (4)$$

where

$$\alpha = L^2 + \frac{K \cdot h_{L'}^2}{W}. \quad (5)$$

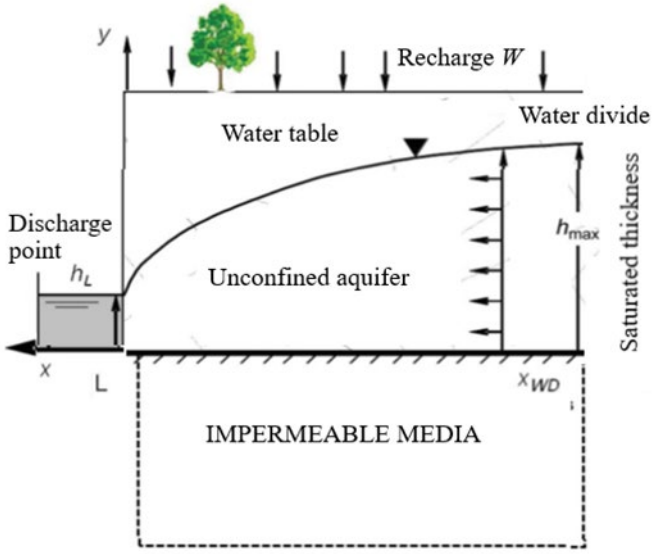

Fig. 2. Conceptual model of flow in a uniformly recharged, unconfined horizontal aquifer, where groundwater flow is unidirectional and unidimensional between the upstream and downstream constant head boundaries. Adapted from (Chesnaux 2013; Chesnaux et al. 2005)

2.5.2. Hydrogeochemical approach

We applied the radioactive decay method (Clark and Fritz 1997) to date groundwater. Dating of groundwater by ^3H decay assumes a known tritium input into the groundwater and that the residual tritium, which is measured in the groundwater sample, is the result of decay. The decay is calculated using Eq. 6.

$$a_t{}^3\mathrm{H} = a_0{}^3\mathrm{H} \times e^{-\lambda t}\,, \tag{6}$$

where $a_0{}^3H$ is the initial tritium activity or concentration (expressed in TU), $a_t{}^3H$ is the activity (measured in a groundwater sample) remaining after decay over time *t*, and λ represents the decay term calculated via Eq. 7, where the half-life $t_{1/2}$ equals 12.43 years.

$$\lambda = \frac{\ln 2}{t_{\frac{1}{2}}}\,. \tag{7}$$

Finally, Eq. 6 can be rewritten as

$$t = -17.93 \times \frac{a_t{}^3\mathrm{H}}{a_0{}^3\mathrm{H}}\,. \tag{8}$$

The value of $a_0{}^3H$ was determined online from a member station of the Global Network of Isotopes in Precipitation (GNIP) database, operated by the International Atomic Energy Agency (Aggarwal et al. 2010). Here, ^3H monthly data are available from August 1953 to March 2019 from the closest GNIP-member station (Ottawa, ON), located approximately 453 km southwest of the study site. The initial tritium concentration ($a_0{}^3H$) data set was chosen to coincide with the recharge potential period suggested by the stable water isotope signatures obtained in this study and to validate the travel time result obtained from the analytical model.

2.5.3. Numerical approach

We applied a numerical-based approach developed using FEFLOW-3D code (Version 7.5) (Diersch 2013). A geological model was initially built using Leapfrog Geo (Seequent 2022) and then integrated within FEFLOW-3D to conduct numerical groundwater flow simulations (Diersch 2013). Numerous studies have confirmed the robustness of these codes (Hudon-Gagnon et al. 2011; Larocque et al. 2019; Nastev et al. 2005).

For these analyses, we modeled the entire 55 ha study area. Maximum depth for the model was 22 m as the natural impermeable substratum has been investigated to this depth. FEFLOW-3D modelling requires information on the horizontal/vertical distribution of hydrofacies to distinguish permeable/impermeable lithofacies within the modeled area. The modeling requires certain input parameters including hydraulic conductivity and porosity. The model is divided into two layers for which the attribution of the hydrogeological parameters is imported as shape files prepared previously in ArcGIS. We selected two layers: (i) the aquifer, assumed as homogeneous, and (ii) the impermeable substratum. The introduced values for hydraulic conductivity and porosity were those obtained from the sieve grain analyses. Once the modelled domain was established, we ran the TetGen mesh generator, included in FEFLOW code, to generate a finite element mesh comprising tetrahedral elements. The steady-state condition was set for the established model, which was constrained by specific boundary conditions. A Dirichlet boundary condition was set by inputting head values on the eastern and western model boundaries. The eastern boundary of the aquifer consisted of a wetland area; this boundary is assumed to be acting as a groundwater divide. The western boundary represents the discharge area where groundwater seeps out of the point of contact between the aquifer and the aquitard, whereas the northern and southern limits of the study site were assigned without any specification. Therefore, these limits were deemed as impermeable borders, as there were no obvious boundaries observed on the field site. The study site was modeled as a domain receiving a uniform spatial recharge, a parameter adopted from the results of the present study, i.e., the groundwater recharge value estimated analytically by the Dupuit–Forchheimer solution.

Model performance based on the available head observations was evaluated with several statistics that rely on the error of the model mass balance and the root mean squared error (RMSE). The RMSE measured the deviation between the simulated and observed water levels within the site`s observation wells and is defined as

$$\mathrm{RMSE} = \sqrt{\frac{\sum_{i=1}^{m} (y_i - O_i)^2}{m}}, \qquad (9)$$

where m is the number of observations, and O_i and y_i are the observed and predicted data, respectively.

The forward particle-tracking option of the FEFLOW-3D code is a postprocessing tool that calculates the pathway and transit time for an introduced particle (Anderson et al. 2015). Particle tracking is generally used for representing the advective transport of solutes and contaminants (Anderson et al. 2015). Here, we applied standard streamlines because they represent trajectories of particles flowing by advective velocity within steady-state conditions; the particle tracking between two specified points corresponds to transit time.

3. Results

3.1. Aquifer stratigraphy from the collected soil samples

The sediment material at the drilled boreholes varied only slightly among sites and matching samples recovered in an earlier study (Courchesne (2019), demonstrating the relative homogeneity of the granular aquifer (Table 2). Samples were dominated by fine to medium/coarse sands with traces of silt and gravel.

344 **Table 2.** Sediment and groundwater characteristics at the drilled boreholes

345

Observation well	Ground elevation (m)	Stratigraphic unit	Elevation at the base of the unit (m)	Water table elevation (m)
S1-BER	179.379	FCBGS-S	171.76	177.63
		CS	171.15	
S2-BER	179.57	FCBGS-S	171.37	177.46
		CS	171.15	
S4-BER	179.88	FCBGS-S	168.30	177.93
		CS	167.69	
PZ-1	182.49	FMGB-S	179.56	180.87
		FCBGS-S	179.19	
PZ-2	180.91	FMGB-S	178.01	179.04
		FCBGS-S	177.10	
PZ-3	180.84	FMGB-S	178.71	179.17
		FCBGS-GS	176.98	
PZ-4	181.34	FMGB-S	177.38	177.96
		FCBGS-GS	176.82	
PZ-5	180.79	FMGB-S	177.79	178.62
		FCBGS-GS	177.22	
PZ-6	181.52	FMGB-S	178.52	179.71
		FCBGS-GS	176.95	
PZ-7	180.19	FMGB-S	176.38	177.61
		FCBGS-GS	175.00	
PZ-9	180.21	FMGB-S	175.33	177.92

346 FCBGS-S, fine to coarse brownish-gray sand with traces of silt; CS, clayey silt; FMGBS-S, fine
347 to medium gray-brownish sand with traces of silt; FCBGS-GS, fine to coarse brownish-gray sand
348 with traces of gravel and silt

349 ### 3.2. Calculated hydrogeological properties
350

351 Grain-size sieve analysis (Fig. 3) using Wentworth's (1922) classification revealed that the
352 aquifer is generally composed of fine to medium/coarse sands with traces of silt and gravel.
353 Using obtained grain-size curves (See in the supplementary material) and estimated soil
354 properties (i.e., porosity and void ratio), we determined the average *Ks* for each combined
355 soil sample. The *Ks* values were calculated using selected empirical equations (Table 1),

and we then averaged the calculated *Ks* to obtain a value *Ks.eq* assumed to represent the entire aquifer. Our obtained *Ks.eq* (4.65×10^{-4} $m \cdot s^{-1}$) was comparable to previous estimates for sites S1 (6.4×10^{-4} $m \cdot s^{-1}$) and S2 (4.5×10^{-4} $m \cdot s^{-1}$) situated in adjacent aquifers (Boumaiza 2008; Boumaiza et al. 2019; Boumaiza et al. 2020b).

After applying the analytical solution (Bear 1972b; Chesnaux 2013), we obtained a quadratic regression of the squared saturated soil height against distance (Fig. 3). The estimated mean groundwater recharge based on a constant parameter—the ratio of recharge to hydraulic conductivity—was 198 mm·year^{-1}. This value is comparable to groundwater recharge assessed within other proximal aquifers in the SLSJ region (Boumaiza et al. 2022b); CERM-PACES (2013).

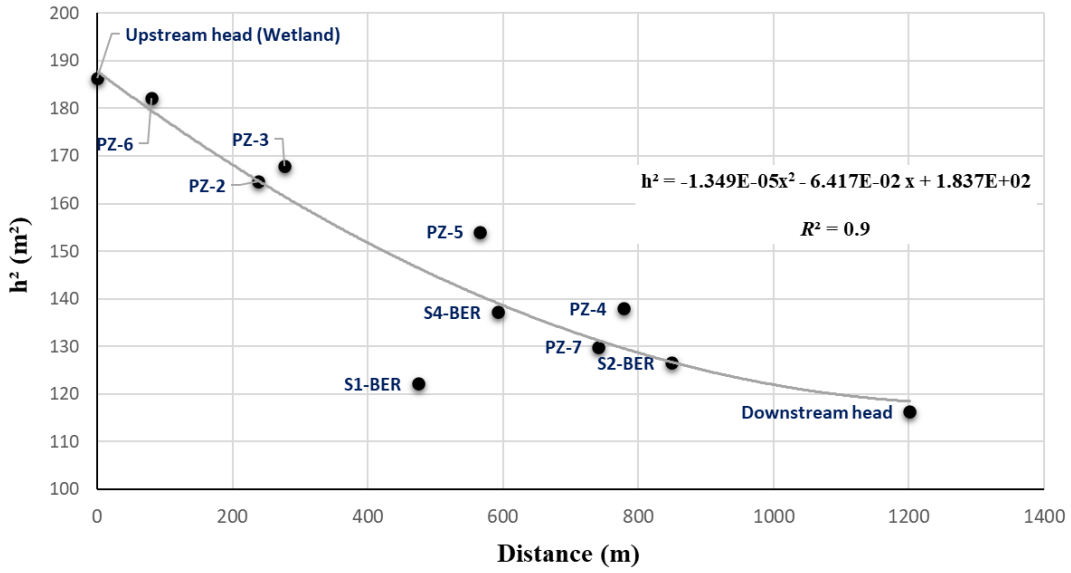

Fig. 3. Quadratic regression of the squared saturated thickness (h^2) along the distance of the cross-section A–A′

The annual (March 2021–March 2022) fluctuations of water table level within the three piezometers at S1-BER, S2-BER and S4-BER (Fig. 4) were integrated into the WTF-ESPERE automated program to estimate mean annual groundwater recharge. The obtained value was 197 mm·year^{-1}, matching the value obtained via the analytical approach. Note that our estimated recharge value of 197 mm·year^{-1} (for the period March 2021–March 2022), accounts for 24.2 % of the annual (March 2021–March 2022) precipitation registered at a station located approximately 1.5 km northeast of the study site indicated a

376 value of 814.5 mm·year^{-1} (Gouv.qc 2022). This value of precipitation is 11 % less than the
377 historical precipitation average value of 916.3 mm·year^{-1} recorded between 2014 and 2021.
378 Consequently, the value of recharge of 197 mm·year^{-1} for the period March 2021–March
379 2022 may slightly underestimate the average historical recharge that would be estimated
380 over the 2014-2021 period. The value of recharge being approximately a quarter of the
381 value of precipitation is expected to be representative of the average regional value of
382 recharge of the aquifer.

383

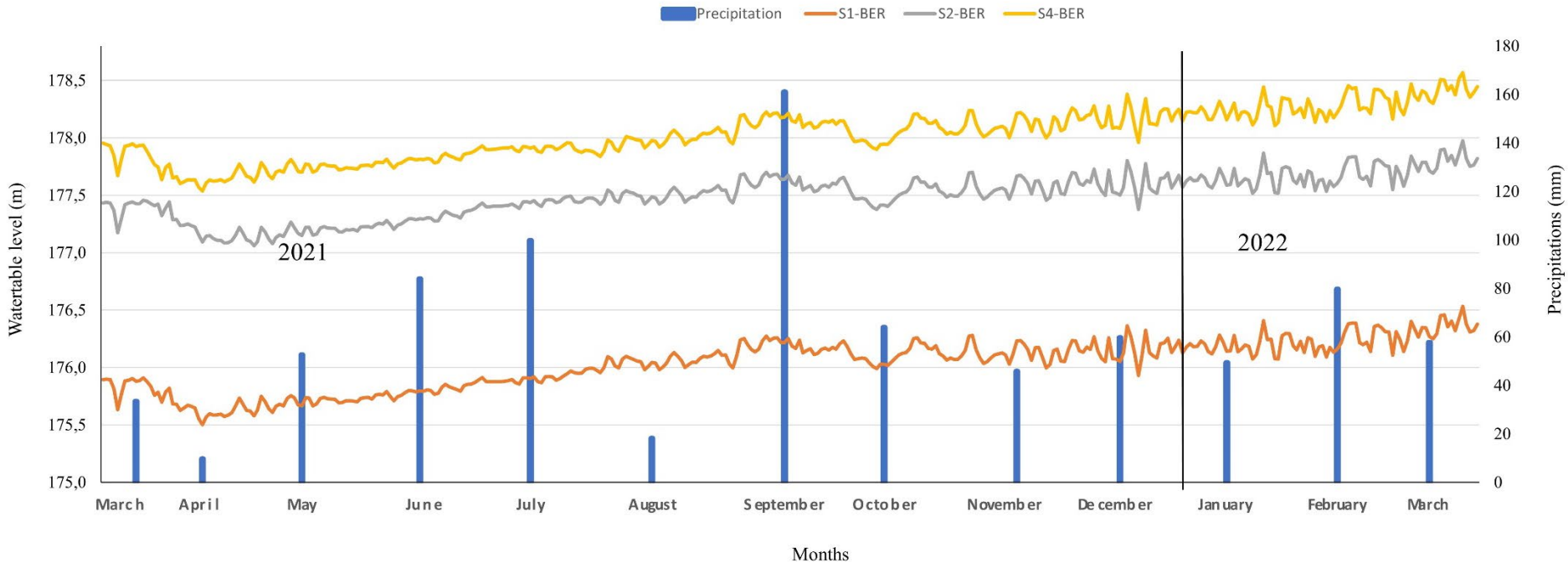

384

385 **Fig. 4.** Elevation of the water table in boreholes S1-BER, S2-BER, and S4-BER and precipitation between March 2021 and March 2022

386

3.3. Groundwater isotopic signatures

The $\delta^{2}H_{H2O}$ and $\delta^{18}O_{H2O}$ values for the collected groundwater samples ranged from −13.76‰ to −9.59‰ with a median value of −11.92‰ for $\delta^{18}O$, and from −98.10‰ to −73.82‰ with a median value of −89.79‰ for $\delta^{2}H$ (Fig. 5). These groundwater isotopic values are comparable to those of Tremblay et al. (2021) who focused on granular aquifers within the Grenville province and St. Lawrence Platform in southern Québec. The range of stable isotope values for $\delta 2H_{H2O}$ and $\delta 18O_{H2O}$ suggests that the water infiltrated the soil during the warm season. This observation is expected for the study site as recharge in northern Quebec occurs during the warmer summer–autumn rather than the colder winter–spring when recharge is negligible because of the presence of a snowpack and frozen surface soil acting as a barrier to water infiltration (Boumaiza et al. 2020a, 2021a; Boumaiza et al. 2021b; Boumaiza et al. 2021c; 2022b; Chesnaux and Stumpp 2018).

When the obtained $\delta^{18}O_{H2O}$ and $\delta^{2}H_{H2O}$ are plotted along the PACES-derived local meteoric water line (LMWL), we note that they plot around the LMWL, suggesting that the groundwater has been recharged into the BER aquifer through the direct infiltration of precipitation with minimal effect from evaporation (Fig. 5). This pattern is expected for the unconfined aquifer of BER that is dominated by permeable sandy material. The S1-BER and PZ-6 groundwater samples plot slightly below the LMWL, reflecting an effect of evaporation or mixing processes. Evaporation appears to be the dominant process because the calculated groundwater d-excess values (d-excess = $\delta^{2}H_{H2O} - 8\delta^{18}O_{H2O}$) for S1-BER (−2.93‰) and PZ-6 (3‰) are low compared with those of S2-BER (11.63‰) and S4-BER (13.9‰), the latter mostly indicative of a modern recharge that is experiencing a reduced evaporation effect. The water table level variations shown in Fig. 4 confirm the warm

410 summer–autumn recharge, as suggested by $\delta^{2}H_{H2O}$ and $\delta^{18}O_{H2O}$ signatures. The plots
411 illustrate an increased water table level beginning in June because of snow melt and rainfall.
412 Consequently, we selected June for the $a_0{}^{3}H$ data set when calculating groundwater transit
413 time via the hydrogeochemical approach.

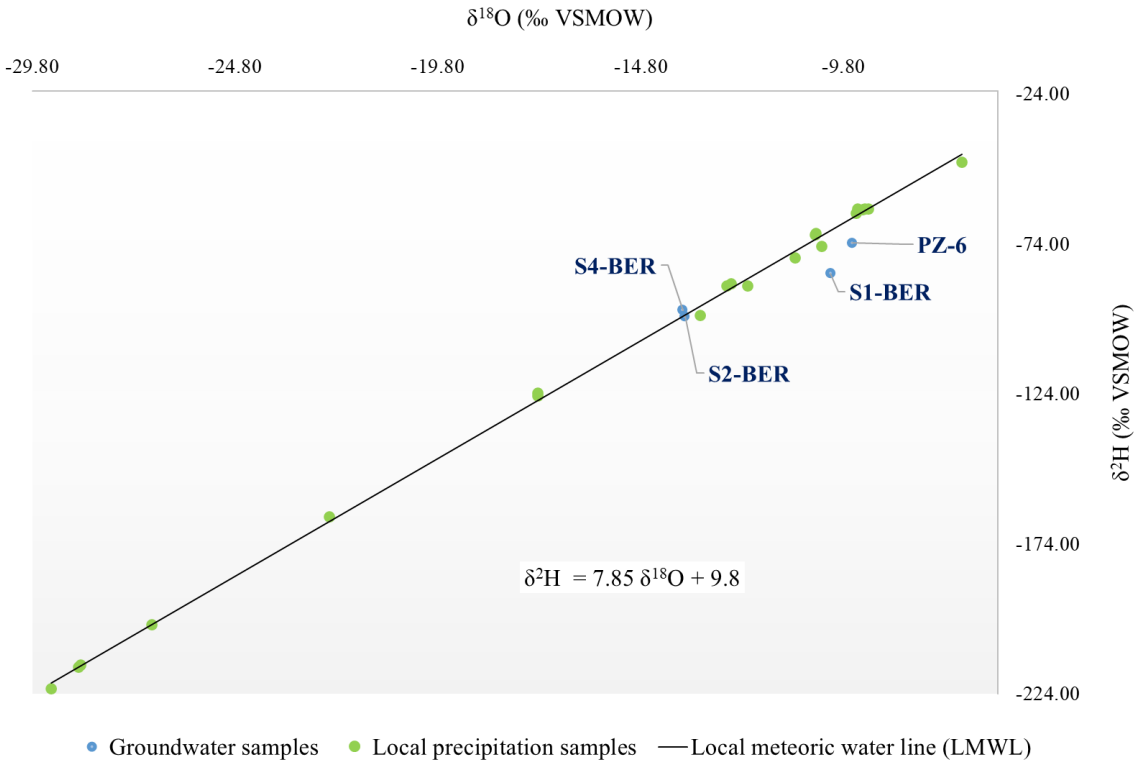

414

415 **Fig. 5.** Distribution of isotopic values of the collected groundwater samples from sites S4-
416 BER, S2-BER, S1-BER, and PZ-6

417 **3.4. Assessed groundwater transit time**

418 *3.4.1. Assessed transit time according to the analytical approach*

419 Because of the homogeneity of the BER aquifer, it is possible to apply the analytical
420 approach to estimate groundwater travel time between the wetland and the discharge zones.
421 We used the analytical solution of Chesnaux et al. (2005) with the upstream head (wetland)
422 and downstream head (discharge point) positioned along a groundwater flow line A–A′
423 (Fig. 1), involving an east–west groundwater flow across the study site. The eastern

boundary condition (wetland) acts as a groundwater divide line, whereas the western imposed boundary represents a groundwater seep (Fig. 2). A groundwater spring was observed at the discharging points during field work. In addition, the studied domain is imposed as homogeneous. Such a flow within the homogeneous sediments of the BER aquifer reflect the Dupuit–Forchheimer flow system conditions, for which groundwater flow is assumed to be under a steady-state regime, unidirectional, and unidimensional within a homogeneous unconfined aquifer constrained by a horizontal substratum. Introducing the calculated mean value of the groundwater recharge into the analytical solution along the A–A′ flow line (Fig. 1), we calculated the groundwater travel time from multiple positions (x_i) to the discharge outlet point (Eq. 4). The calculated groundwater travel time from wetland to the discharge point was approximately 7.75 years, with a relatively consistent time vs. tracking distance along the A–A′ flow line (Fig. 6).

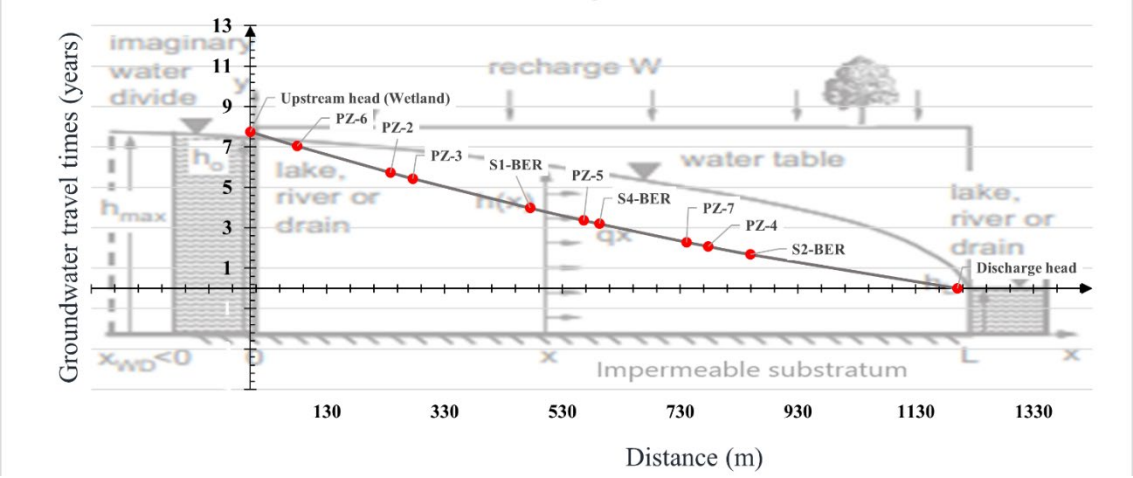

Fig. 6. Illustration of groundwater transit times in the BER aquifer in relation to distance. Background illustration adapted from (Chesnaux et al. 2005)

3.4.2. Assessed transit time according to the hydrogeochemical approach

The obtained activities of ^{3}H ($a_t{}^{3}H$) from the collected groundwater samples are presented in Table 3. The initial ^{3}H activity ($a_0{}^{3}H$) was set at 9.2 TU, measured from precipitation collected 15 June 2014, a representative month for the potential groundwater recharge period as suggested by $\delta^{2}H_{H2O}$ and $\delta^{18}O_{H2O}$ (i.e., starting from June), and a year (2014) reflecting the transit time yielded by the analytical approach (7.75 years). We calculated the transit times by applying the radioactive decay calculation method (Eq. 8) to the groundwater sample signatures (Table 3). Because we did not have a sample representing the discharge head directly, we considered S2-BER (located at 351 m from the discharge boundary) as the discharging point. We calculated a transit time from the wetland (recharging point) to the discharging point (S2-BER) of 7.34 years.

Table 3. Tritium activity and groundwater travel times computed using the hydrogeochemical approach

Sample	$a_t{}^{3}H$ (tritium units)	Date of $a_t{}^{3}H$	$a_0{}^{3}H$ (tritium units)	Date of $a_0{}^{3}H$	Transit time (years)
PZ-6	9	2021-12-10	9.2	2014-06-15	0.31
S2-BER	6.1	2021-12-14	9.2	2014-06-15	7.34
S4-BER	6.5	2021-12-14	9.2	2014-06-15	6.09

Tritium is reported in tritium units; 1TU = 3.221 $pCi \cdot L^{-1}$

3.4.3. Assessed transit time according to the numerical approach

Our calibration of the numerical model generated a model mass balance of 1.64×10^{-2} %, and the calculated RMSE was 0.31 m, highlighting the robustness of the fitting process between the simulated and the observed water level data (Fig. 7)

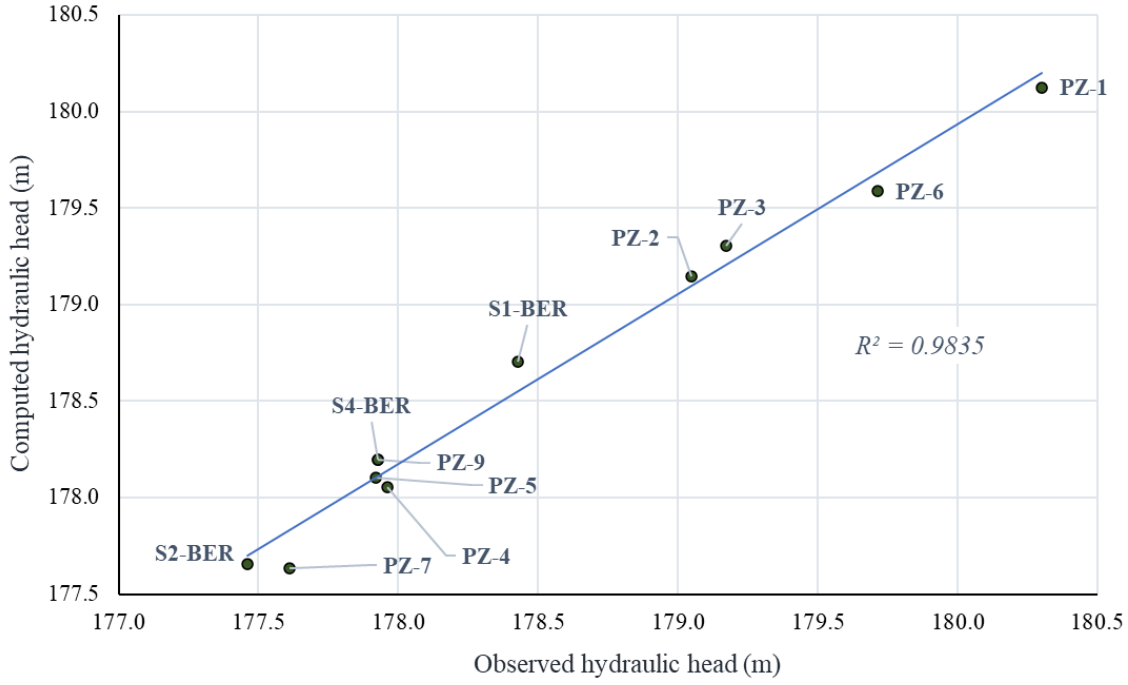

458

459 **Fig. 7.** Relationship between the observed and computed hydraulic heads (m)

460 Once calibrated, the model computed the transit time for a particle tracking in the forward

461 direction, i.e., from the wetland to discharge point along the groundwater A–A′ flow line,

462 as presented in Fig. 8. We calculated a transit time of 7.27 years through this approach.

463

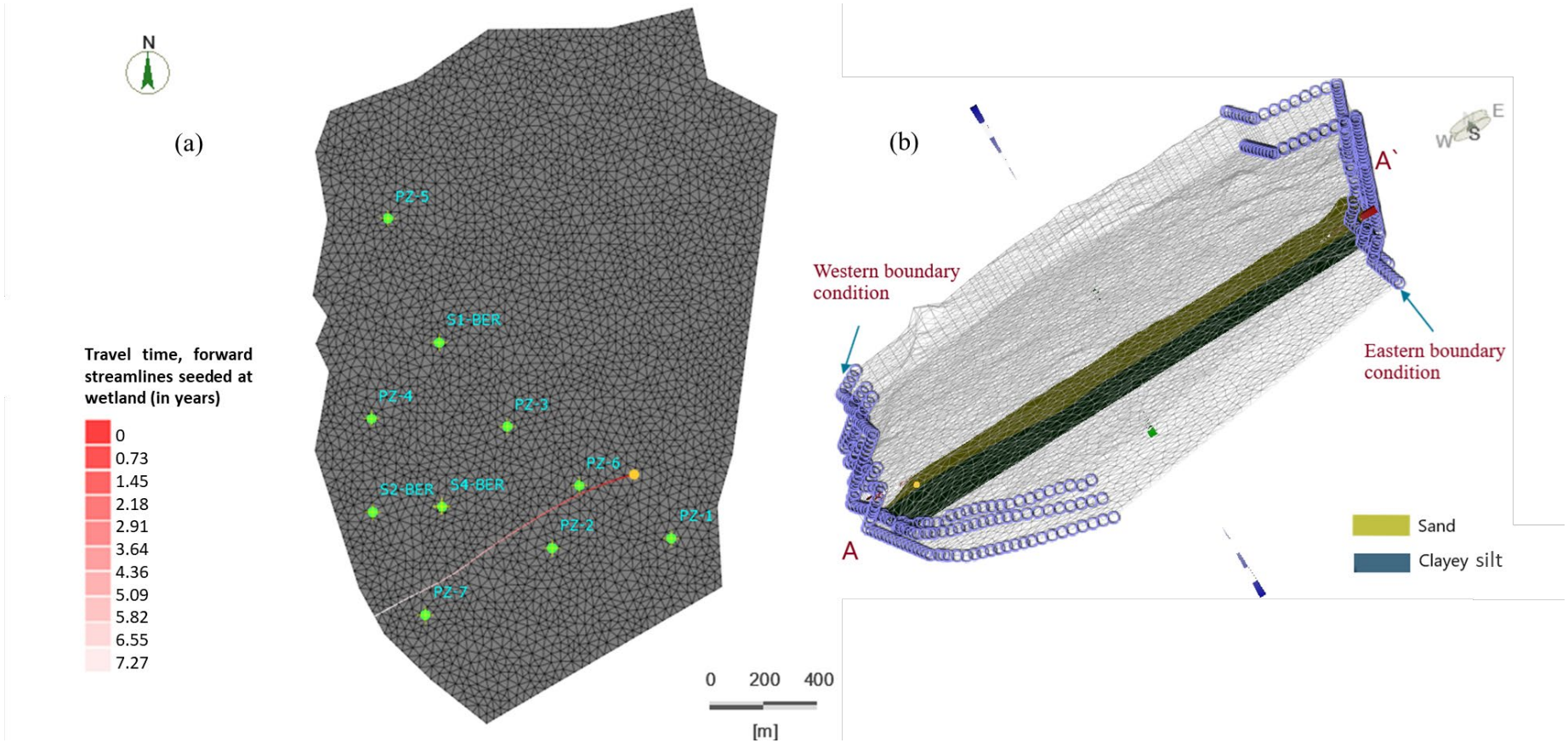

Fig. 8. (a) A 1D representation of the domain modeled by using the FEFLOW model. The traced line is the tracking path, and the transit time in years is indicated in the legend; (b) a 3D perspective of the studied aquifer

468 **Discussion**

469 Estimates of transit time using the analytical approach involve a number of limitations.
470 These limitations include the uncertainty associated with the input parameters (for use of
471 Eq. 4), including hydraulic conductivity, groundwater recharge, and porosity. Furthermore,
472 the restrictive assumptions associated with a Dupuit–Forchheimer flow type aquifer
473 produce simplistic albeit realistic features of the study site. For instance, contaminant
474 transport is affected by multiple natural processes (Bradley 2013; Gorelick et al. 1993) and
475 can be subjected to diverse transportation processes, e.g., diffusion and dispersion, rather
476 than only advection as assumed in our study. Moreover, infiltration through the vadose
477 zone can influence groundwater transit time (Boumaiza et al. 2021a), whereas our
478 analytical and numerical approaches limit groundwater flow to only the saturated zone.
479 Thus, the assessed groundwater transit time using the our analytical and numerical
480 approaches is less certain. Sousa et al. (2013) and Wang et al. (2012) demonstrated that
481 aquifers having a thick vadose zone exhibit a much longer groundwater transit time in this
482 zone; for example(Schwientek et al. 2009; Zoellmann et al. 2001) found that unsaturated
483 zones greater than 10 m thick affected groundwater transit times. Given that the BER site
484 has a thin unsaturated zone (0.5–2 m), we believe any vadose zone effects on transit time
485 are negligeable.

486 The hydrogeochemical approach determined that the groundwater transit time was 7.34
487 years, slightly less than that obtained via the analytical method (7.75 years). This subtle
488 difference may stem from S2-BER being considered as the discharge point. This point is
489 350 m distant from the actual downstream head boundary, as considered in the analytical
490 model. Moreover, ^{3}H activity and the associated transit times (Table 3) agree with

491 published values. Indeed, Clark and Fritz (1997) indicate that for continental regions, as is
492 the case of our study site, ^{3}H concentrations between 5 and 15 TU correspond to modern
493 recharge (<5–10 years).

494 Nonetheless, the hydrogeochemical approach relies on a simple model, which is not a
495 typical characteristic of natural systems. This approach assumes that three samples are
496 sufficient for obtaining an accurate transit time, and this approach does not consider
497 possible mixing processes during the recharge and infiltration (Michel 2005). As shown by
498 Małoszewski et al. (1983) and Vitvar and Balderer (1997), the use of isotopes and solutes
499 is limited by short data time series, which provides little insight into the temporal variation
500 of transit times. Moreover, because the ^{3}H concentrations of remnant bomb pulse waters in
501 the Northern Hemisphere are currently greater than concentrations in modern rainfall, it is
502 increasingly necessary to estimate transit times using ^{3}H-level time series (Morgenstern et
503 al. 2010). (Clark and Fritz 1997) recommend to ideally use a ^{3}H input representing a
504 multiyear average and applying an input function calculated via a model that incorporates
505 mixing and decay into the recharge process.

506 The numerical approach yielded a transit time of 7.27 years, slightly shorter than that of
507 the analytical and hydrogeochemical approaches. A source of error in the numerical
508 approach involves uncertainties and insufficiencies in the input data. Although these
509 inputed parameters are the same as those of the analytical approach, it appears that the
510 calibrating process involving a change in these input parameters affects the estimated
511 transit time.

512 Furthermore, advection is also assumed to be the main transport mechanism for our
513 particle-tracking computation. Therefore, in cases where dispersion is expected to play an
514 important role, our approach may not be very applicable. However, in terms of contaminant
515 transport, this method is suited for conservative solutes because other biogeochemical
516 reactions are not explicitly considered.

517 Moreover, actual aquifer depths recorded during field observations were used in the
518 FEFLOW 3D model. Therefore, the 3D model does not present a perfectly horizontal
519 substratum as assumed by the Dupuit–Forchheimer system. This difference could explain
520 the variation between the two results. In the analytical model, we assumed that the saturated
521 thickness of the aquifer was uniform. This assumption does not necessarily reflect the
522 actual geological conditions. Indeed, the base of the aquifer forms a slight slope (Figs. 1
523 and 8b), leading to a variable saturated zone thickness. Because the thickness of the
524 saturated aquifer affects both the transit path track and the horizontal hydraulic gradients
525 (Haitjema 1995), the longer transit time estimated by the analytical approach, relative to
526 that of the numerical approach, can be attributed to uncertainties in the initial estimates of
527 saturated aquifer thickness. This discrepancy demonstrates the challenge in considering a
528 representative saturated thickness for an unconfined aquifer, especially at larger scales.
529 Therefore, the analytical solution proposed by Chesnaux et al. (2005) appears valid under
530 conditions of an idealized unconfined aquifer with a slight variation in head relative to the
531 saturated aquifer thickness.

532 All three methods required significant amounts of field data. The analytical approach was
533 the least complex and the least time-consuming once these data were available, whereas

534 the numerical approach required the most time investment to learn the software and
535 involved laborious computational resources. Finally, the geochemical approach was of
536 intermediate complexity because of the waiting period for the results, although their
537 interpretation was not time consuming. Consequently, if the main goal is the approximate
538 and prompt estimation of transit time, the analytical solution provides the best approach.

539 **3. Conclusion and discussion**

540 We combined analytical, hydrogeochemical, and numerical approaches in a multi-
541 technique framework to estimate advective groundwater transit time in granular
542 unconfined aquifer. Transit time represented the time for groundwater to be transported
543 from a wetland to the discharge zone of the aquifer. We integrated realistic soil physical
544 properties into the analytical and numerical approaches and used ^{3}H-groundwater isotopes
545 in the hydrogeochemical approach. Estimated groundwater transit times varied from 7.27
546 to 7.75 years for the three approaches, demonstrating the advantage of combining several
547 approaches using field data to estimate groundwater transit time. Further studies are
548 required to estimate groundwater transit time through the vadose zone; these results would
549 allow tracking groundwater movement from the ground surface to the discharge point.

550 Our study aimed to estimate the transit time of potential contamination generated from an
551 agricultural field to the nearby river, using groundwater transit time as analog of
552 contaminant transit time and assuming a simple transport advective mechanism. Additional
553 studies should consider other processes affecting contaminant transport, such as dispersion,
554 diffusion, sorption, and degradation. Nonetheless, our study provides a valuable
555 contribution to understanding the behaviour of the BER aquifer and to improving the

management of groundwater resources of this aquifer. Also, it can be underlined that the methodology applied in our study could be applied to larger aquifers where high-resolution field data cannot be collected. In this case, it is suggested to use remote sensing data such as satellite imagery, or geophysical data that can provide information on larger areas in aquifers. This data can be used to calibrate models and validate the results (Lévesque et al., 2023). Finally, while high-resolution field data may not be obtained for the entire aquifer, it may be possible to collect data at a few strategic locations that can be representative of a larger extent of the aquifer.

Acknowledgments

The authors thank Mitacs Globalink Graduate Fellowship Program,Canada (IT17061), *Fonds d'appui au rayonnement des régions* (FARR), and *Fondation de l'Université du Québec à Chicoutimi* (FUQAC) for financial support. The authors also thank David Noël for his greatly appreciated help and guidance during field work and Mike Bellemare, Laura-Pier Perron Desmeules, and Pier-Olivier Gilbert for their assistance during field work.

Declaration of interests

☒ The authors declare that they have no known competing financial interests or personal relationships that could have appeared to influence the work reported in this paper.

☐ The authors declare the following financial interests/personal relationships which may be considered as potential competing interests.

577

578

579 Aggarwal, P.K., Araguás-Araguás, L.J., Groening, M., Kulkarni, K.M., Kurttas, T., Newman, B.D.,
580 and Vitvar, T. 2010. Global hydrological isotope data and data networks. Isoscapes: 33-
581 50.
582 Anderson, M.P., Woessner, W.W., and Hunt, R.J. 2015. Chapter 8 - Particle Tracking. *In* Applied
583 groundwater modeling: simulation of flow and advective transport. Academic press.
584 Basu, N.B., Jindal, P., Schilling, K.E., Wolter, C.F., and Takle, E.S. 2012. Evaluation of analytical
585 and numerical approaches for the estimation of groundwater travel time distribution.
586 Journal of Hydrology, **475**: 65-73.
587 Bear, J. 1972a. Dynamics of fluids in porous media. American Elsevier Publishing Company, New
588 York, NY.
589 Bear, J. 1972b. Dynamics of Fluids in Porous Media. No. pties. 1 à 2. American Elsevier Publishing
590 Company.
591 Bear, J. 1988. Dynamics of fluids in porous media. Courier Corporation.
592 Bethke, C.M., and Johnson, T.M. 2008. Groundwater age and groundwater age dating. Annual
593 Review of Earth and Planetary Sciences, **36**: 121-152.
594 Beyer, W. 1964. Zur Beschreibung der Wasserdurchlässigkeit von Kiesen und Sanden. Zeitschr. f.
595 Wasserwirtschaft-Wassertechnik, **14**: 165-168.
596 Black, C.A. (ed). 1965. Methods of soil analysis. Pt. 1. Physical and mineralogical properties,
597 including statistics of measurement and sampling. American Society of Agronomy,
598 Madison, WI.
599 Boumaiza, L. 2008. Caractérisation hydrogéologique des hydrofaciès dans le paléodelta de la
600 rivière Valin au Saguenay. Université du Québec à Chicoutimi.
601 Boumaiza, L., Rouleau, A., and Cousineau, P. Estimation de la conductivité hydraulique et de la
602 porosité des lithofaciès identifiés dans les dépôts granulaires du paléodelta de la rivière
603 Valin dans la région du Saguenay au Québec. *In* Proceedings of the 68th Canadian
604 Geotechnical Conference, Quebec City, Quebec, Canada. p. 2015. Vol. 9.
605 Boumaiza, L., Rouleau, A., and Cousineau, P. Determining hydrofacies in granular deposits of the
606 Valin River paleodelta in the Saguenay region of Quebec. *In* Proceedings of the 70th
607 Canadian Geotechnical Conference and the 12th Joint CGS/IAH-CNC Groundwater
608 Conference, Ottawa, Ontario, Canada. 2017. Vol. 8.
609 Boumaiza, L., Rouleau, A., and Cousineau, P. Combining shallow hydrogeological
610 characterization with borehole data for determining hydrofacies in the Valin River
611 paleodelta. *In* Proceedings of the 72nd Canadian Geotechnical Conference, St-John's,
612 Newfoundland, Canada. p. 2019. Vol. 8.
613 Boumaiza, L., Chesnaux, R., Walter, J., and Stumpp, C. 2020a. Assessing groundwater recharge
614 and transpiration in a humid northern region dominated by snowmelt using vadose-
615 zone depth profiles. Hydrogeology Journal, **28**: 2315-2329.
616 Boumaiza, L., Chesnaux, R., Walter, J., and Stumpp, C. 2020b. Assessing groundwater recharge
617 and transpiration in a humid northern region dominated by snowmelt using vadose-
618 zone depth profiles. Hydrogeology Journal : Official Journal of the International
619 Association of Hydrogeologists, **28**: 2315-2329. doi:10.1007/s10040-020-02204-z.
620 Boumaiza, L., Chesnaux, R., Walter, J., and Stumpp, C. 2021a. Constraining a flow model with
621 field measurements to assess water transit time through a vadose zone. Groundwater,
622 **59**: 417-427.

623 Boumaiza, L., Chesnaux, R., Walter, J., and Meghnefi, F. 2021b. Assessing response times of an
624 alluvial aquifer experiencing seasonally variable meteorological inputs. Groundwater for
625 Sustainable Development, **14**: 100647.
626 Boumaiza, L., Chesnaux, R., Walter, J., Lenhard, R.J., Hassanizadeh, S.M., Dokou, Z., and Alazaiza,
627 M.Y. 2022a. Predicting vertical LNAPL distribution in the subsurface under the
628 fluctuating water table effect. Groundwater Monitoring & Remediation, **42**: 47-58.
629 Boumaiza, L., Chesnaux, R., Drias, T., Walter, J., Huneau, F., Garel, E., Knoeller, K., and Stumpp,
630 C. 2020c. Identifying groundwater degradation sources in a Mediterranean coastal area
631 experiencing significant multi-origin stresses. Science of the Total Environment, **746**:
632 141203.
633 Boumaiza, L., Walter, J., Chesnaux, R., Brindha, K., Elango, L., Rouleau, A., Wachniew, P., and
634 Stumpp, C. 2021c. An operational methodology for determining relevant DRASTIC
635 factors and their relative weights in the assessment of aquifer vulnerability to
636 contamination. Environmental Earth Sciences, **80**: 1-19.
637 Boumaiza, L., Walter, J., Chesnaux, R., Lambert, M., Jha, M.K., Wanke, H., Brookfield, A.,
638 Batelaan, O., Galvão, P., and Laftouhi, N.E. 2022b. Groundwater recharge over the past
639 100 years: Regional spatiotemporal assessment and climate change impact over the
640 Saguenay-Lac-Saint-Jean region, Canada. Hydrological Processes, **36**: e14526.
641 Bradley, P. 2013. Current Perspectives in Contaminant Hydrology and Water Resources
642 Sustainability.
643 Cartwright, I., and Morgenstern, U. 2015. Transit times from rainfall to baseflow in headwater
644 catchments estimated using tritium: the Ovens River, Australia. Hydrology and Earth
645 System Sciences, **19**: 3771-3785.
646 Cartwright, I., and Morgenstern, U. 2016. Using tritium to document the mean transit time and
647 sources of water contributing to a chain-of-ponds river system: implications for resource
648 protection. Applied Geochemistry, **75**: 9-19.
649 CERM-PACES. 2013. Résultats du programme d'acquisition de connaissances sur les eaux
650 souterraines du Saguenay-Lac-Saint-Jean. Université du Québec à Chicoutimi
651 Chapuis, R.P. 2004. Predicting the saturated hydraulic conductivity of sand and gravel using
652 effective diameter and void ratio. Canadian Geotechnical Journal, **41**: 787-795.
653 Chesnaux, R. 2013. Regional recharge assessment in the crystalline bedrock aquifer of the
654 Kenogami Uplands, Canada. Hydrological Sciences Journal, **58**: 421-436.
655 Chesnaux, R., and Stumpp, C. 2018. Advantages and challenges of using soil water isotopes to
656 assess groundwater recharge dominated by snowmelt at a field study located in Canada.
657 Hydrological Sciences Journal, **63**: 679-695.
658 Chesnaux, R., Molson, J., and Chapuis, R. 2005. An analytical solution for ground water transit
659 time through unconfined aquifers. Groundwater, **43**: 511-517.
660 Chesnaux, R., Marion, D., Boumaiza, L., Richard, S., and Walter, J. 2021. An analytical
661 methodology to estimate the changes in fresh groundwater resources with sea-level rise
662 and coastal erosion in strip-island unconfined aquifers: illustration with Savary Island,
663 Canada. Hydrogeology Journal, **29**: 1355-1364.
664 Clark, I.D., and Fritz, P. 1997. Environmental isotopes in hydrogeology. FL, Boca Raton. pp. 328
665 p. : illustrations ; 26 cm.
666 Cook, P.G., and Böhlke, J.-K. 2000. Determining timescales for groundwater flow and solute
667 transport. *In* Environmental tracers in subsurface hydrology. Springer. pp. 1-30.
668 Cook, P.G., and Herczeg, A.L. 2012. Environmental tracers in subsurface hydrology.
669 Cornaton, F. 2003. Deterministic models of groundwater age, life expectancy and transit time
670 distributions in advective-dispersive systems. Université de Neuchâtel.

Courchesne, C. 2019. Caractérisation hydrogéologique de la bleuetière d'enseignement et de recherche Secteur Normandin, Québec. Université du Québec à Chicoutimi, Chicoutimi.
Diersch, H.-J.G. 2013. FEFLOW: finite element modeling of flow, mass and heat transport in porous and fractured media. Springer Science & Business Media.
Dupuit, J.E. 1863. Etudes théoriques et pratiques sur le mouvement des eaux dans les canaux découverts et à travers les terrains perméables avec des considérations relatives au régime des grandes eaux, au débouché à leur donner, et à la marche des des alluvions dans les rivières à fond mobile. Dunod, éditeur.
Ekwurzel, B., Schlosser, P., Smethie Jr, W.M., Plummer, L.N., Busenberg, E., Michel, R.L., Weppernig, R., and Stute, M. 1994. Dating of shallow groundwater: Comparison of the transient tracers 3H/3He, chlorofluorocarbons, and 85Kr. Water Resources Research, **30**: 1693-1708.
Etcheverry, D., and Perrochet, P. 2000. Direct simulation of groundwater transit-time distributions using the reservoir theory. Hydrogeology Journal, **8**: 200-208.
Fontes, J.-C. 1992. Chemical and isotopic constraints on 14 C dating of groundwater. *In* Radiocarbon after four decades. Springer. pp. 242-261.
Forchheimer, P. 1886a. Uber die Ergiebigkeit von Brunnenanlagen and Sickershlitzen. **32**.
Forchheimer, P. 1886b. Uber die Ergiebigkeit von Brunnenanlagen and Sickershlitzen. Z. Architect Ing. Verein, Hannover, **32**.
Gardner, W.H. 1965. Water content. Methods of Soil Analysis: Part 1 Physical and Mineralogical Properties, Including Statistics of Measurement and Sampling, **9**: 82-127.
Gillon, M., Barbecot, F., Gibert, E., Plain, C., Corcho-Alvarado, J.-A., and Massault, M. 2012. Controls on 13C and 14C variability in soil CO2. Geoderma, **189**: 431-441.
Goode, D.J. 1996. Direct simulation of groundwater age. Water Resources Research, **32**: 289-296.
Gorelick, S.M., Freeze, R.A., Donohue, D., and Keely, J.F. 1993. Groundwater contamination: optimal capture and containment. Lewis Publishers Inc.
Gouv.qc. 2022. Normales climatiques du Québec 1981-2010 [accessed 2021-02-10.
Haitjema, H.M. 1995. Analytic element modeling of groundwater flow. Elsevier.
Hazen, A. 1983. Some physical properties of sand and gravel with special reference to their use in filtration. 24th Ann, Rep., Mass. State Board of Health, Boston, 1983.
Healy, R.W., and Cook, P.G. 2002. Using groundwater levels to estimate recharge. Hydrogeology Journal, **10**: 91-109.
Hudon-Gagnon, E., Chesnaux, R., Cousineau, P.A., and Rouleau, A. 2011. A methodology to adequately simplify aquifer models of quaternary deposits: preliminary results. GeoHydro 2011.
Labrecque, G.v., Chesnaux, R., and Boucher, M.-A.l. 2020. Water-table fluctuation method for assessing aquifer recharge: application to Canadian aquifers and comparison with other methods. Hydrogeology Journal, **28**.
Lanini, S., and Caballero, Y. 2021. ESPERE, a Tool for Multimethod Aquifer Recharge Estimation: What's New with Version 2? Groundwater, **59**: 5-6.
Lanini, S., Caballero, Y., Seguin, J.-J., and Maréchal, J.-C. 2016. ESPERE-A multiple-method Microsoft Excel application for estimating aquifer recharge. Groundwater, **54**: 155-156.
Larocque, M., Levison, J., Martin, A., and Chaumont, D. 2019. A review of simulated climate change impacts on groundwater resources in Eastern Canada. Canadian Water Resources Journal/Revue canadienne des ressources hydriques, **44**: 22-41.
LaSalle, P., and Tremblay, G. 1978. Dépôts meubles Saguenay-Lac-Saint-Jean.

718 Lefebvre, K., Barbecot, F., Larocque, M., and Gillon, M. 2015. Combining isotopic tracers (222Rn
719 and δ13C) for improved modelling of groundwater discharge to small rivers.
720 Hydrological Processes, **29**: 2814-2822.
721 Leray, S., De Dreuzy, J.-R., Bour, O., Labasque, T., and Aquilina, L. 2012. Contribution of age data
722 to the characterization of complex aquifers. Journal of Hydrology, **464**: 54-68.
723 Lévesque, Y., Chesnaux, R. and Walter, J. 2023. Using geophysical data to assess groundwater
724 levels and the accuracy of a regional numerical flow model. Hydrogeology Journal, **31**:
725 351-370.
726 Małoszewski, P., Rauert, W., Stichler, W., and Herrmann, A. 1983. Application of flow models in
727 an alpine catchment area using tritium and deuterium data. Journal of Hydrology, **66**:
728 319-330.
729 Mazariegos, J.G., Walker, J.C., Xu, X., and Czimczik, C.I. 2017. Tracing artificially recharged
730 groundwater using water and carbon isotopes. Radiocarbon, **59**: 407-421.
731 Mazor, E. 2003. Chemical and isotopic groundwater hydrology. CRC press.
732 McCarthy, J., and Zachara, J. 1989. ES&T Features: Subsurface transport of contaminants.
733 Environmental science & technology, **23**: 496-502.
734 McGuire, K.J., and McDonnell, J.J. 2006. A review and evaluation of catchment transit time
735 modeling. Journal of Hydrology, **330**: 543-563.
736 Michel, R.L. 2005. Tritium in the hydrologic cycle. *In* Isotopes in the water cycle. Springer. pp. 53-
737 66.
738 Milan, V., and Andjelko, S. 1992. Determination of hydraulic conductivity of porous media from
739 grain-size composition. No. 551.49 V 986.
740 Morgenstern, U., Stewart, M.K., and Stenger, R. 2010. Dating of streamwater using tritium in a
741 post nuclear bomb pulse world: continuous variation of mean transit time with
742 streamflow. Hydrology and Earth System Sciences, **14**: 2289-2301.
743 Nastev, M., Rivera, A., Lefebvre, R., Martel, R., and Savard, M. 2005. Numerical simulation of
744 groundwater flow in regional rock aquifers, southwestern Quebec, Canada.
745 Hydrogeology Journal, **13**: 835-848.
746 Navfac, D. 1974. Design manual-soil mechanics, foundations, and earth structures. US
747 Government Printing Office, Washington, DC.
748 Nimmo, J.R., Horowitz, C., and Mitchell, L. 2015. Discrete-storm water-table fluctuation method
749 to estimate episodic recharge. Groundwater, **53**: 282-292.
750 Penna, D., Stenni, B., Šanda, M., Wrede, S., Bogaard, T., Gobbi, A., Borga, M., Fischer, B.,
751 Bonazza, M., and Chárová, Z. 2010. On the reproducibility and repeatability of laser
752 absorption spectroscopy measurements for δ 2 H and δ 18 O isotopic analysis.
753 Hydrology and Earth System Sciences, **14**: 1551-1566.
754 Ritter, K.S., Paul Sibley, Ken Hall, Patricia Keen, Gevan Mattu, Beth Linton, Len. 2002. Sources,
755 pathways, and relative risks of contaminants in surface water and groundwater: a
756 perspective prepared for the Walkerton inquiry. Journal of Toxicology and
757 Environmental Health Part A, **65**: 1-142.
758 Sauerbrey, I. 1932. On the problem and determination of the permeability coefficient.
759 Proceedings VNIIG: 115-145.
760 Schwientek, M., Maloszewski, P., and Einsiedl, F. 2009. Effect of the unsaturated zone thickness
761 on the distribution of water mean transit times in a porous aquifer. Journal of
762 Hydrology, **373**: 516-526.
763 Seequent. 2022. Leapfrog Geo 2021.2.5 Help and Support. Available from
764 https://www.seequent.com/help-support/leapfrog-geo/ [accessed 01-15 2022].

765 Sousa, M.R., Jones, J.P., Frind, E.O., and Rudolph, D.L. 2013. A simple method to assess
766 unsaturated zone time lag in the travel time from ground surface to receptor. Journal of
767 contaminant hydrology, **144**: 138-151.
768 Taylor, C. 1976. Tritium enrichment of environmental waters by electrolysis: development of
769 cathodes exhibiting high isotopic separation and precise measurement of tritium
770 enrichment factors.
771 Tremblay, R., Walter, J., Chesnaux, R., and Boumaiza, L. 2021. Investigating the Potential Role of
772 Geological Context on Groundwater Quality: A Case Study of the Grenville and St.
773 Lawrence Platform Geological Provinces in Quebec, Canada. Geosciences, **11**: 503.
774 Vitvar, T., and Balderer, W. 1997. Estimation of mean water residence times and runoff
775 generation by180 measurements in a Pre-Alpine catchment (Rietholzbach, Eastern
776 Switzerland). Applied Geochemistry, **12**: 787-796.
777 Vogel, J. 1967. Investigation of groundwater flow with radiocarbon: in Isotopes in Hydrology:
778 International Atomic Energy Agency. Vienna.
779 Wang, L., Stuart, M., Bloomfield, J., Butcher, A., Gooddy, D., McKenzie, A., Lewis, M., and
780 Williams, A. 2012. Prediction of the arrival of peak nitrate concentrations at the water
781 table at the regional scale in Great Britain. Hydrological Processes, **26**: 226-239.
782 Wentworth, C.K. 1922. A scale of grade and class terms for clastic sediments. The journal of
783 geology, **30**: 377-392.
784 Zappa, G., Bersezio, R., Felletti, F., and Giudici, M. 2006. Modeling heterogeneity of gravel-sand,
785 braided stream, alluvial aquifers at the facies scale. Journal of Hydrology, **325**: 134-153.
786 Zedler, J.B., and Kercher, S. 2005. Wetland resources: status, trends, ecosystem services, and
787 restorability. Annu. Rev. Environ. Resour., **30**: 39-74.
788 Zoellmann, K., Kinzelbach, W., and Fulda, C. 2001. Environmental tracer transport (3H and SF6)
789 in the saturated and unsaturated zones and its use in nitrate pollution management.
790 Journal of Hydrology, **240**: 187-205.

791